

Robust Deep Multi-Modal Sensor Fusion using Fusion Weight Regularization and Target Learning

Myung Seok Shim, Chenye Zhao, Yang Li, Xuchong Zhang, Wenrui Zhang, and Peng Li

Abstract—Sensor fusion has wide applications in many domains including health care and autonomous systems. While the advent of deep learning has enabled promising multi-modal fusion of high-level features and end-to-end sensor fusion solutions, existing deep learning based sensor fusion techniques including deep gating architectures are not always resilient, leading to the issue of fusion weight inconsistency. We propose deep multi-modal sensor fusion architectures with enhanced robustness particularly under the presence of sensor failures. At the core of our gating architectures are fusion weight regularization and fusion target learning operating on auxiliary unimodal sensing networks appended to the main fusion model. The proposed regularized gating architectures outperform the existing deep learning architectures with and without gating under both clean and corrupted sensory inputs resulted from sensor failures. The demonstrated improvements are particularly pronounced when one or more multiple sensory modalities are corrupted.

Index Terms—Deep Learning, Sensor Fusion, Autonomous Systems.

I. INTRODUCTION

Sensor fusion is a key to many applications such as autonomous systems equipped with multiple sensing modalities [1]. For instance, inputs from cameras and LIDARs are fused with deep neural networks [2–6]. Inertial measurement units and other sensors are employed for activity recognition on portable devices, and various fusion techniques for activity recognition have been proposed [7].

A. Related Work

Specifically, [3] presents a convolutional neural network (CNN) approach to sensor fusion in autonomous driving and compares three fusion schemes: early, late, and deep fusion. However, this work does not consider sensor failures and provides no deep insight on computational principles of sensor fusion. The typical late fusion DNN architecture is shown in

Myung Seok Shim is with the Department of Electrical and Computer Engineering, Texas A&M University, College Station, TX, 77843, USA (e-mail: shim.myungseok@tamu.edu).

Chenye Zhao is with the Department of Electrical and Computer Engineering, University of Illinois at Chicago, 851 S Morgan St, Chicago, IL 60607, USA (email: czhao43@uic.edu)

Yang Li was with the Department of Electrical and Computer Engineering, Texas A&M University, College Station, TX, 77843, USA (e-mail: li13157@tamu.edu)

Xuchong Zhang is with the School of Electronic and Information Engineering Xi'an Jiaotong University, Xianning West Road, Xi'an, Shaanxi, 710049, P.R. China (email: zhangxc@stu.xjtu.edu.cn)(The work was performed during his visit to Texas A&M University.)

Wenrui Zhang and Peng Li are with the Department of Electrical and Computer Engineering, UC Santa Barbara, Santa Barbara, CA 93106, USA (e-mail: wenruizhang@ucsb.edu, lip@ucsb.edu)(corresponding author: Peng Li)

Fig. 1 (a) where each modality is first processed, e.g. by a number of convolutional/pooling/activation layers. And then all extracted feature maps are fused together, e.g. by element-wise mean at the layer marked by “+”, and processed further to make the final decision.

A key objective and challenge in sensor fusion is attaining *resilience*, i.e., the fusion task shall be conducted robustly not only under clean sensory inputs but also in the presence of sensor failures. [8], [9], and [10] display CNN based object tracking with input weighting (gating) fusion scheme and auxiliary losses. By weighting more important input channel with fusion weights (gating factors) which are processed with a sigmoid function, the weighted important inputs have more effect on outputs and the classification accuracy is further improved.

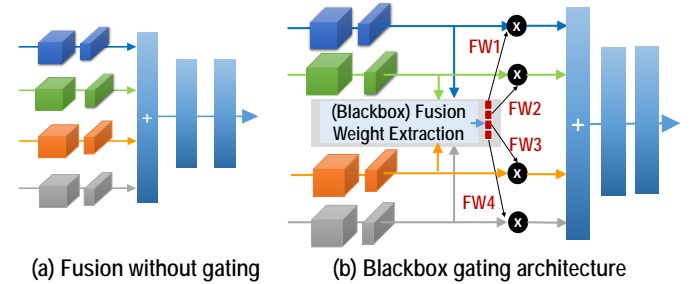


Fig. 1: Two DNN sensor fusion architectures.

As another example of gating architectures, [5] proposes a gated convolutional neural network called *NetGated* architecture, where two fusion weights which are extracted from the camera and LIDAR inputs are employed to multiply the corresponding pre-processed camera/LIDAR features, respectively, in order to compute a weighted sum of the two. The weighted sum passes through fully connected layers to produce the final robot steering command. This gating architecture is illustrated for the case of four sensory modalities in Fig. 1(b), where four scalar fusion weights (FW1 to FW4) are extracted by fusing the pre-processed feature maps of the four modalities.

Comparing with a non-gating architecture like the one in Fig. 1(a), gating architectures (e.g. Fig. 1(b)) are positioned to provide a more structured fusion solution. Interference from a highly noisy or failing sensor can be completely gated off simply when the corresponding extracted fusion weight is zero, a desirable property hard to be implemented in a non-gating architecture.

B. Limitations of the existing gating architectures

Gating architectures such as NetGated extract a fusion weight (map) for each sensory input [5, 6, 11]. Ideally, the fusion weights shall reflect the integrity and importance of the corresponding modalities w.r.t. the classification task. It is desirable to gate off a corrupted modality by a small or zero-valued fusion weight. However, the end-to-end black-box nature of these architectures can lead to *fusion weights inconsistency*. Fusion weights which are extracted by the NetGated [5] tend to be unstable and fail to consistently reflect the importance of modalities, leading to observed poor performance. There are cases where the Netgated architecture even underperforms non-gating architectures. Furthermore, gating architectures with the auxiliary losses [8, 9] which are handled in each auxiliary input channel regularize main CNN model. Though this regularization scheme improves overall performance, how it regularizes the fusion weight is not touched. Because this fusion weight regularization may resolve fusion weight inconsistency issue with target fusion weight learning, the classification accuracy might be further improved.

C. Main contributions

We present a new gating architecture and its variants with significantly improved performance and resilience under both clean sensory inputs and sensor failures. Our main contributions are: **1)** propose a new auxiliary-model regulated gating architecture, called *ARGate*, to robustly learn gating fusion weights of different modalities using auxiliary unisensory processing paths during training; **2)** As part of the ARGate architecture, propose two regularization techniques, namely, *fusion weight regularization with auxiliary losses*, and *monotonic fusion target learning* to regularize fusion weights with corresponding auxiliary losses and target for consistent fusion weights in the training process and significantly improve the performance and robustness; and **3)** shed light on the fusion and regularization mechanisms that are responsible for the observed performance improvements.

We perform comprehensive evaluation of the proposed ARGate architectures while comparing with a baseline non-gating CNN architecture and the NetGated architecture [5] utilizing the Human Activity Recognition (HAR) dataset [12], driver identification dataset [13], and KITTI dataset [14] under various sensory input conditions. It is demonstrated that the proposed architectures consistently outperform the baseline and NetGated architectures, and improve classification accuracy by up to 8.49% and 13.39% over the baseline and NetGated architectures, respectively. For the KITTI dataset, the proposed architecture outperforms a reference architecture [2] by up to 4.81%.

II. OVERVIEW OF THE ARGATE ARCHITECTURES

The ARGate architecture with the two most essential regularization techniques, i.e. *fusion weight regularization with auxiliary losses* and *monotonic fusion weight target learning*, is depicted in Fig. 2.

Multisensory processing has been under extensive study in neuroscience and recent research has shed increasing light on

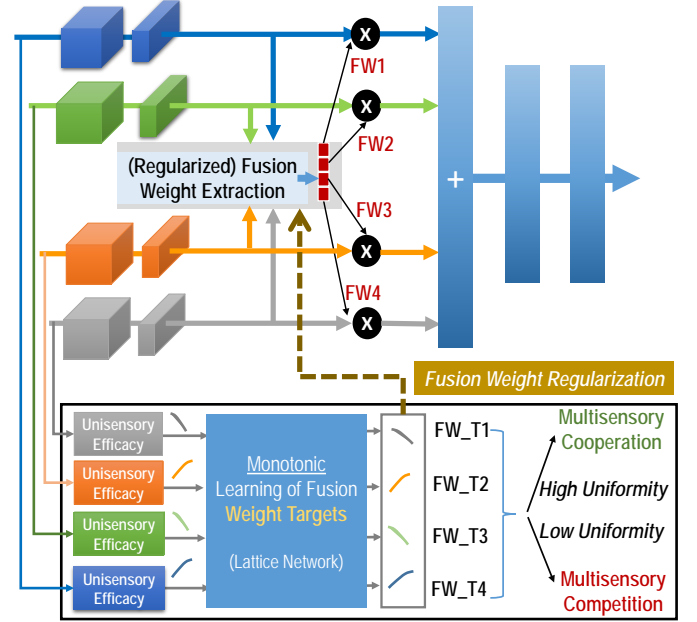


Fig. 2: ARGate architecture with fusion weight regularization and monotonic fusion weight target learning. The bottom box offers fusion weight regulation for training the main model (upper portion) and is removed for inference.

the computational mechanisms underlying the multi-sensory processing of superior colliculus (SC) neurons in the mid-brain [15, 16], providing a relevant reference for the proposed ARGate architectures. Animals must promptly select the most pertinent modalities while suppressing spurious noise from other senses for their survival, where *multisensory competition* plays an essential role. This is analogous to the targeted robust sensor fusion problem under catastrophic sensor failures. On the other hand, mature SC neurons are able to enhance their performance via *multisensory cooperation* where congruent stimuli across modalities are integrated. This corresponds to performance benefits in the targeted sensor fusion brought by fusing co-variant and complementary sensory inputs.

As such, multisensory competition and cooperation may be considered as two intertwined operating modes, transitions between which may be orchestrated based on sensory conditions: operate in competition when inputs are non-congruent (e.g. due to strong sensory noise or catastrophic failures) to ensure robustness while switching to cooperation to maximize performance with clean/covariant inputs.

Loosely speaking, the proposed architecture in Fig. 2 (a detailed full implementation is in Fig. 4) bears high-level resemblance to mode transitions in SC neurons suggested by the electrophysiological recording and computational studies [15]. However, it takes a rather different strategy to balance between multisensory competition and cooperation in the end-to-end deep learning architecture during training. The bottom block of Fig. 2 outputs the fusion weight targets (FW_T1 to FW_T4), which are used to regularize the fusion weight extraction block such that each fusion weight FW_i is constrained to be near the corresponding target FW_Ti. This acts as a solution to the fusion weight inconsistency problem of the typical gating

architectures.

The key idea here is to transparently balance between multi-sensory competition and cooperation by detecting the efficacy (i.e. conditioning or importance) of each unisensory input for the same end prediction task. The efficacy is evaluated by the training loss of a “unisensory efficacy” block, which is essentially a unisensory model for the same task with the corresponding modality being the sole input. Intuitively, a high unisensory efficacy shall be mapped to a high fusion weight target value. To allow for a flexible end-to-end architecture, the efficacies are mapped to the fusion weight targets (FW_T1 to FW_T4) by a trainable monotonic lattice network ensuring the monotonic relationship between the two. Since fusion weight targets sum up to 1.0, low uniformity among fusion weight targets immediately leads to multisensory competition where the inputs with smaller fusion weight targets tend to be depressed. High uniformity in the fusion weight targets would give rise to multisensory cooperation where modalities with similar fusion target values are integrated in a balanced way. The design of the ARGate architectures is detailed as follows.

III. THE PROPOSED ARGATE ARCHITECTURE

A. Basic structure of ARGate

As a first step, we present a primitive ARGate architecture with weight sharing (ARGate-WS), which is enclosed in a more complete version of the ARGate architecture called ARGate+ in Fig. 3. The ARGate+ architecture will be built upon ARGate-WS and explained in the next subsection.

For ease of discussion, we assume that there exist two sensory inputs as in Fig. 3. To assist the training of the main model, which is employed for inference, an auxiliary (aux) model is included. The main model is architecturally similar to the NetGated architecture. When splitting the output of the “FC-con” layer into the fusion weights, we further introduce sigmoid and a softmax function to normalize the fusion weights between [0,1], so that the importance of input features are expressed with the magnitude of the fusion weights.

In general, the aux model consists of multiple independent auxiliary paths, one for each modality without fusion. The weight parameters in the convolutional layers and early FC layers are shared between the corresponding modalities across the main and aux models. The total training loss is a weighted sum of the losses of the main model and all auxiliary paths. The adopted weight sharing (WS) is illustrated by the dashed purple box in Fig. 3. Weight sharing is commonly used in the literature [3, 8]. Here, it acts as a way of regularizing the main model.

Based on this primitive ARGate-WS architecture only with weight sharing, we explore the more complete ARGate+ architecture with two fusion weight regularization techniques next.

B. Fusion Weight Regularization with Auxiliary Losses: ARGate+ Architecture

When one or more sensory channels are completely corrupted, weight sharing in ARGate-WS fails to properly regularize the corresponding convolutional/FC layers for the

corrupted input channels in the main model. This is because that these auxiliary paths can no longer be trained to deliver a good performance based on the single corrupted modality.

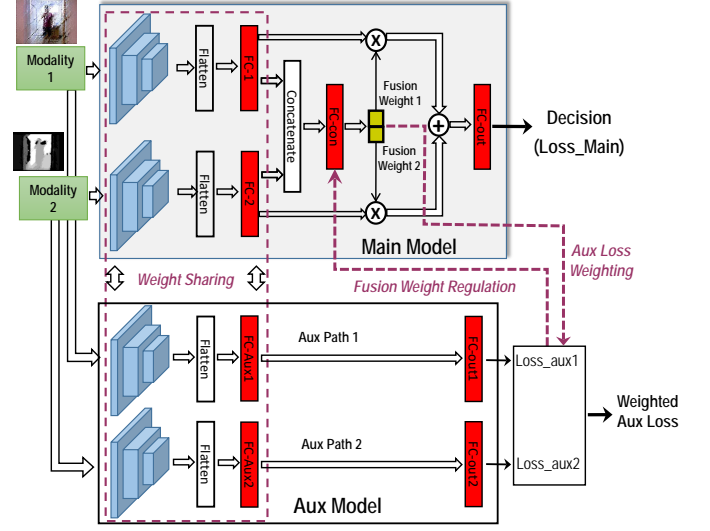


Fig. 3: The proposed ARGate+ architecture

Our key observation is that the losses of different auxiliary paths reflect the relevance of these modalities w.r.t. to the classification task, and hence, can be used for *fusion weight regularization* (FWR), which is depicted using a purple dashed line pointing from the aux model to the main model in Fig. 3. When a particular sensory modality is corrupted under an input example, the high loss of its auxiliary path will constrain the training of the “FC-con” layer in the main model to produce a low fusion weight for that modality.

Since the loss of each auxiliary path is included in the total training loss, the large loss of any corrupted sensory input can be dominant, potentially lowering performance. To resolve this problem, we use the extracted fusion weights from the main model as the corresponding weights of the auxiliary losses in the total training loss. We call this scheme auxiliary loss weighting (ALW) as shown by the dashed purple line pointing from the main model to the aux model in Fig. 3. This leads to a more complete ARGate+ architecture with a new loss function:

$$Loss = Loss_{main} + \alpha \cdot \sum_{k=1}^K w_{fusion}^k Loss_{aux}^k + \beta \cdot \sum_{k=1}^K \left(w_{fusion}^k - e^{-\widehat{Loss_{aux}^k}} \right)^2 \quad (1)$$

where the auxiliary path loss $Loss_{aux}^k$ is weighted by the fusion weight w_{fusion}^k , hence the dominance of any large auxiliary path loss resulted from sensor failures is diminished.

Each normalized auxiliary-path loss $e^{-\widehat{Loss_{aux}^k}}$ is employed to regularize w_{fusion}^k . Here, $e^{-\widehat{Loss_{aux}^k}}$ is obtained by plugging $Loss_{aux}^k$ into the exponential function and then normalizing $e^{-\widehat{Loss_{aux}^k}}$ using sigmoid and then softmax normalization so that $e^{-\widehat{Loss_{aux}^k}}$ is between [0,1].

With above-mentioned explanation, the last term of the right hand side of (1) is directly used as fusion weight targets for regularizing the fusion weights of the main model. The ARGate+ architecture integrates weight sharing (WS), fusion weight regularization with auxiliary losses (FWR), and auxiliary loss weighting (ALW). Next, we discuss the other key proposed technique, namely, monotonic fusion target learning.

C. Monotonic Fusion Target Learning

Regularizing fusion weight through auxiliary losses is a key step towards improving the overall performance. Notice that the last term in (1) implements fusion weight regularization in which the exponential of each normalized auxiliary path is called the fusion weight target for the corresponding fusion weight. While this specific form of fusion weight targets pushes the training of the network towards producing a low fusion weight value for modalities with a large auxiliary path loss, the optimal mapping from the auxiliary path loss to the corresponding fusion weight target is not known *a priori*. Our key idea is to optimize this mapping end-to-end as part of the overall network architecture based on the available training data.

Since the fusion weight target of an auxiliary path shall be a *monotonically* non-increasing function of the corresponding auxiliary path loss, this motivates us to introduce a dedicated small network to learn the mapping from the set of auxiliary path losses $\vec{Loss}_{aux} = [Loss_{aux}^1, Loss_{aux}^2, \dots, Loss_{aux}^K]^T$ to each fusion weight target $w_{fusion,t}^k: w_{fusion,t}^k = f_k(\vec{Loss}_{aux})$. Corresponding, the loss is modified from (1) to:

$$Loss = Loss_{main} + \alpha \cdot \sum_{k=1}^K w_{fusion}^k Loss_{aux}^k + \beta \cdot \sum_{k=1}^K \left(w_{fusion}^k - f_k(\vec{Loss}_{aux}) \right)^2. \quad (2)$$

The mappings from the auxiliary losses to the fusion weight targets may be learned with great flexibility by a generic feed-forward multi-layer neural network. However, this approach is not robust due to lack of regularization. We propose to embed a regularized deep lattice network (DLN) [17] to the ARGate+ architecture for more robust learning of fusion targets. As illustrated in Fig. 5, a lattice network can learn input-to-output mappings while guaranteeing the user-specified full or partial monotonicity between the a set of the inputs and outputs.

Integrating a DLN network into ARGate+ leads to a new architecture called ARGate-L in Fig. 4. In general, DLNs consist of three types of layers: calibrators, linear embeddings, and lattices, all of which can be constrained to obey partial or full monotonicity between selected inputs and outputs. Linear embedding layers map the inputs linearly to the outputs. Monotonicity between a subset of inputs/outputs can be forced by choosing non-negative coefficients between them. A lattice is a linearly interpolated multi-dimensional look-up table; each output of the lattice can be constrained to be monotonic in a subset of the inputs. Calibrators are 1-d lattices and can nonlinearly transform a single input and may be used

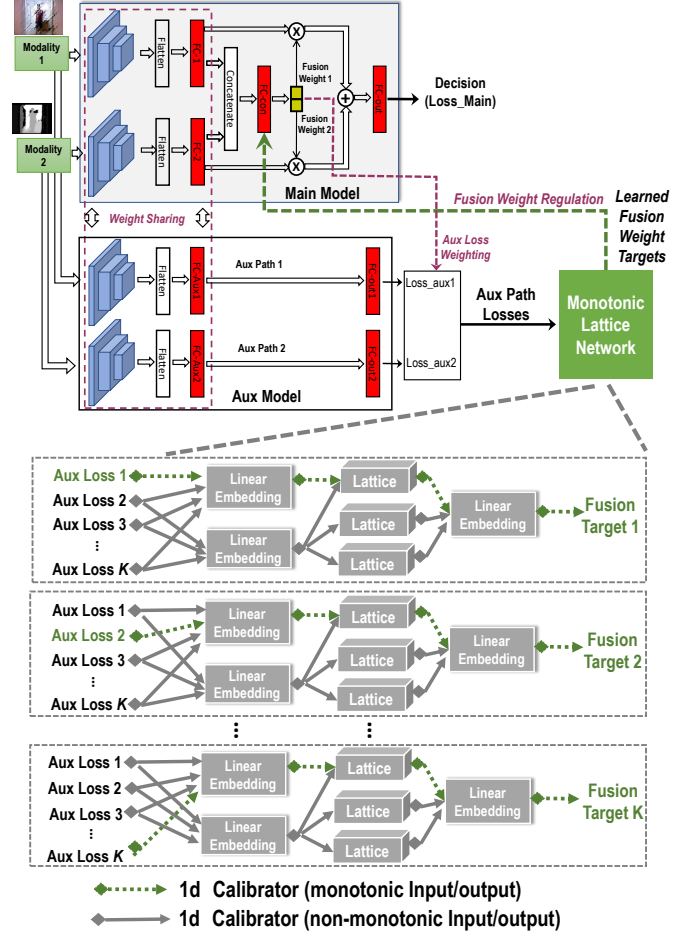


Fig. 4: The proposed ARGate-L architecture with end-to-end monotonic learning of fusion targets using a lattice network.

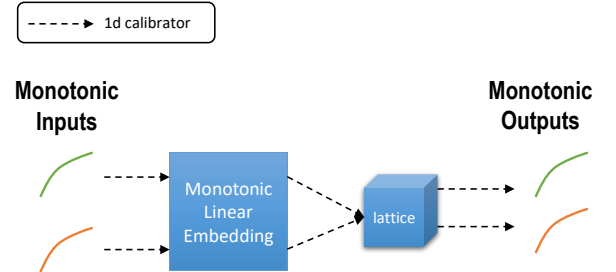


Fig. 5: Learning of monotonic input-output mappings.

for pre-processing and normalization between layers in the DLN.

The proposed lattice network is illustrated in Fig. 4 for the general case of mapping K auxiliary path losses to the corresponding K fusion targets. In its most general form, this can be done by having K independent subnetworks, one for each fusion target. While a particular architecture is chosen for each subnetwork in Fig. 4, in practice, it can be simplified/optimized to suit a given application. The key idea in the proposed lattice network design is to ensure the partial monotonicity between each pair of auxiliary loss and fusion target; there are K

such constraints. In the lattice network of Fig. 4, monotonic inputs/outputs are processed by a calibrator in dashed green while non-monotonic ones are processed by a calibrator in solid gray. The output of a component is monotonic if any of its inputs is monotonic to ensure the end-to-end monotonicity between a pair of auxiliary loss and fusion targets. Specifically, there exist a green dashed path from each auxiliary loss k to its corresponding fusion target k . Imposing these monotonicity constraints acts as a regularization mechanism, making the robust end-to-end learning of fusion weight targets possible and leading to improved performance as we demonstrate later.

IV. EXPERIMENTAL SETTINGS

We perform comprehensive comparison of a non-gating fusion CNN baseline [3], the NetGated architecture [5], and variants of the proposed ARGate architecture on the HAR [12], driver identification [13], and KITTI [14] datasets.

A. Datasets

1) *The Human Activity Recognition Dataset*: The Human Activity Recognition (HAR) dataset [12] includes six activities to be recognized: walking, walking upstairs, walking downstairs, sitting, standing, and laying. From accelerometer and gyroscope, nine sensory inputs are utilized for experiments, where each sensory input is distributed between $[-1, 1]$. There are 7,352 examples for training and 2,947 examples for testing.

2) *The Driver Identification Dataset*: The driver identification dataset [13] consists of 10 drivers' cruising data collected by a CarbigP OBD-II scanner. There are 51 features in total, but 15 features are used in our experiments which is same experimental setup from the original paper. 75,501 training and 18,879 testing examples are used.

3) *KITTI Dataset*: In the KITTI dataset [14], there are two sensory inputs: a RGB image and a velodyne laser scanned bird eye view (BEV) image. The provided 7481 training frames are split into a training and a validation set. For evaluation with detecting the *car* class in images, we adopt the easy, moderate and hard difficulty-level settings provided by KITTI.

B. Neural Network Configurations

1) *Configurations for the HAR and Driver Identification Datasets*: In the HAR and driver identification datasets, the non-gating CNN baseline, NetGated, and the proposed ARGate variants are compared. The late fusion scheme is utilized in the CNN baseline. For fair comparison, tunable parameters of all neural networks are closely matched.

2) *Configurations for the KITTI Dataset*: **AVOD Baseline**. We use the Aggregate View Object Detection (AVOD) approach [2] as a baseline.

AVOD-ARGate. We embed our ARGate-L into the AVOD, specifically in the region proposal network(RPN) as shown in Fig. 6. Feature maps from each input are passed into small ARGate block to produce fusion weights which are regularized by a lattice network. Outputs from these FC layers are added and passed onto the *fusion* block (a FC layer) to create the

fusion weights. These fusion weights are multiplied with the corresponding feature maps from the outputs of the 1×1 feature extracting layers. Furthermore, the fusion weights from RPN is utilized again as gating factors for each modality in the second stage fusion(AVOD) to fortify the network robustness. For target fusion weight learning, the lattice architecture (Cal-Lin-Cal-Lat) is used with the linear embedding layers processing two input channels and one lattice. The total number of tunable parameters of the AVOD baseline and AVOD-ARGate are closely matched for fair performance comparisons. Moreover, since AVOD based algorithms need plane data for training and test, we utilize plane data provided by AVOD for training set, and custom plane data for test set for fair comparison.

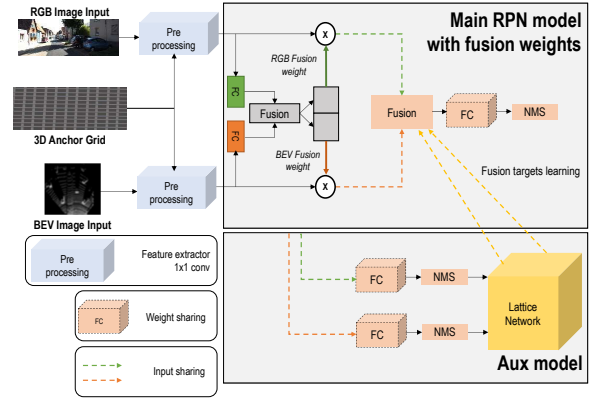


Fig. 6: The proposed ARGate architecture with RPN model for training.

C. Sensor Failures

Apart from using the clean data in the HAR and driver identification datasets, we introduce sensor failures and set up various training/testing sets to comprehensively compare the robustness/generalization of different architectures.

1) *Modeling of failing sensors*: All clean scalar inputs are normalized to be within $[-1, 1]$. We use two schemes: *uniform*, and *Gaussian*, to model a failing sensor by setting its input values respectively to pure noise following a uniform distribution between $[-1, 1]$, and pure noise following the Gaussian distribution $\mathcal{N}(0, 1)$.

2) *Corrupted examples for training/testing*: For HAR and driver identification datasets, we use clean and corrupted examples in both the training and test sets, where in each set $\frac{1}{3}$ of the examples are randomly chosen and kept clean while the remaining ones are corrupted by one or more failing sensors using one of the approaches described below.

Fixed Failing Sensor Assignment. This mimics the situation in which a number of sensors have failed permanently. We select $n_{f, \text{clean}}$ channels out of a total of n sensors to be clean and assume that all remaining sensors have permanent failure when setting up the corrupted examples of for both the training and test sets in each experiment.

Random Failing Sensor Assignment. To more closely mimic random nature of sensor failures, for each corrupted example in the training/test set, we randomly select n_{rclean} channels out of all n sensors to be clean and corrupt the remaining channels. As such, sensors that have failed may vary from one example to another. n_{fclean} and n_{rclean} are varied to for different severity levels of failures.

Failing Sensor Generation Test. This tests model generation by using a test set containing corrupted examples which have a larger or different number of failing sensors from the corrupted examples used to train the model, i.e. the test set has examples with a severe level of sensor failure.

V. EVALUATION

A. Quality of Fusion Weight Extraction

To shed some light on the fusion mechanisms of the NetGated, ARGate-WS and the proposed ARGate+ architectures, we examine the distributions of the trained fusion weight of the sensory input $total_acc_y$ under the HAR dataset. If the $total_acc_y$ is corrupted, then the fusion weight of itself should be distributed lower than the fusion weight of clean $total_acc_y$. Please note that ARGate-WS only utilizes weight sharing so that we compare our proposed ARGate+ with ARGate-WS in terms of fusion weight regularization. The sensor failures are modeled using the random failing sensor assignment with uniform distribution and with $n_{rclean} = 1$ so that 8 out of 9 sensory inputs are corrupted in each example. To show the effects of sensor failures on the fusion weights, we split the examples into two subsets: one in which $total_acc_y$ is corrupted with 8 other inputs and the other subset where $total_acc_y$ is the only clean input. Fig. 7(a, b, c) displays the fusion weight distributions of the first subset for the three architectures while Fig. 7(d, e, f) shows those of the second subset.

One may expect that, in a properly trained model, the fusion weight value for a corrupted sensory modality shall be much smaller than when the modality is clean. However even when $total_acc_y$ is corrupted, Fig. 7(a, b, c) show that the $total_acc_y$ fusion weight distribution of the NetGated architecture has a peak around the large value of 0.4 which is not presented in the case of ARGate-WS. The distribution of ARGate-WS has a much reduced mass on large fusion weight values compared to that of the NetGated. Furthermore, the fusion weight value can go beyond 0.4 in NetGated and ARGate-WS while it is pretty much constrained between 0.06 and 0.1 in ARGate+. One also expects that the fusion weight of $total_acc_y$ shall be large for the second subset since $total_acc_y$ is the only clean input. However, as seen in Fig. 7d, the distribution of NetGated has a large population mass on low fusion weight values. The population mass on low fusion weight values gets reduced significantly in the case of ARGate-WS Fig. 7e, which is further reduced in ARGate+ for which most fusion weights are distributed between 0.33 and 0.45 as shown in Fig. 7f.

B. Results on the HAR Dataset

[Fixed Failing Sensor Assignment] We consider two cases where the number of clean input channels n_{fclean}

is set to 5 and 6, respectively. When $n_{fclean} = 5$, $body_total_acc_x$, $body_acc_x$ and $body_gyro_x$ are corrupted and set to uniform-ally distributed noise while $body_acc_z$ and $body_gyro_y$ are corrupted by uniform-ally distributed noise when $n_{fclean} = 6$. Table II shows that our proposed ARGate architectures outperform the CNN and NetGated significantly while adopting the lattice network in ARGate-L further improves over ARGate+.

[Random Failing Sensor Assignment] In Table I compares the baseline CNN, NetGated, ARGate-WS, proposed ARGate+, and ARGate-L architectures with the number of randomly chosen clean sensors $n_{rclean} \in \{1, 5, 8\}$. When all channels are clean, NetGated has 0.44% prediction accuracy improvement over the baseline while ARGate+, and ARGate-L outperform the baseline by 1.63%, and 2.65%, respectively. ARGate architectures always have better accuracy than the baseline and NetGated, and in general ARGate+ further improves over ARGate-WS which only employs weight sharing (WS) between the main and auxiliary model, demonstrating the effect of fusion weight regularization with auxiliary losses (FWR). ARGate-L is the best-performing model, which incorporates WS, FWR, and the lattice network for monotonic fusion weight target learning. With $n_{rclean} = 1$ and sensor failures which are modeled using uniformly distributed noise, ARGate-L outperforms the baseline, NetGated, ARGate-WS, and ARGate by 7.57%, 6.73%, 3.94%, and 2.54%, respectively. We expect that the performance improvements of the ARGate architectures may be attributed to their improved quality in the fusion weight target learning.

[Failing Sensor Generation Test] In Table III, the first column specifies the numbers of randomly chosen failing channels used in the training and test sets. For example, (1,2)(3,8) means that the number of failing sensors for training are randomly picked from [1,2] while the range of the failing sensors for testing is [3,8]. Essentially, we evaluate the generalization of the models by including corrupted examples with more failing channels in the test set than in the training set. Failing sensors are modeled using uniformly distributed noise. NetGated can underperform the baseline while ARGate-L always outperforms the baseline and NetGated by upto 5.17% and 5.37%, respectively.

C. Results on the Driver Identification Dataset

[Fixed Failing Sensor Assignment] In Table IV, the corrupted inputs are set to uniformly distributed noise. When $n_{fclean} = 5$, *Long Term Fuel Trim Bank1*, *Maximum indicated engine torque*, *Calculated LOAD value*, *Activation of Air compressor*, and *Engine coolant temperature* are corrupted. When $n_{fclean} = 7$, two more input channels, *Intake air pressure* and *Fuel consumption* are corrupted. ARGate-L significantly outperforms the other two models. When $n_{fclean} = 5$, ARGate-L improves over the baseline and NetGated by 8.25% and 6.27%, respectively.

[Random Failing Sensor Assignment] In Table V, different models with the number of randomly selected clean channels $n_{rclean} \in \{5, 8, 12\}$ are compared. When all 15 input channels are clean, the proposed ARGate-L improves

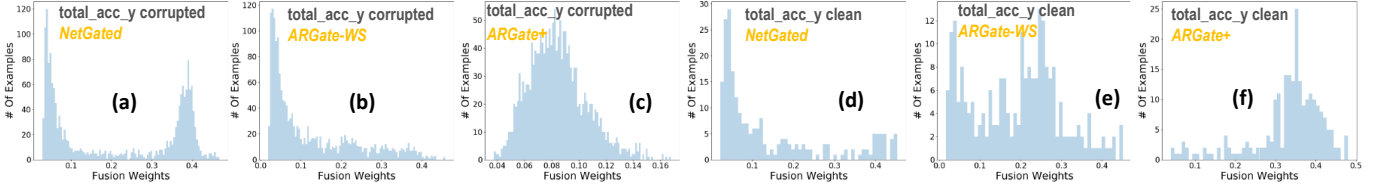


Fig. 7: Fusion weight distributions of the clean or corrupted channel total_acc_y extracted by NetGated, ARGate-WS and ARGate+ under random failing sensor assignment with $n_{rclean} = 1$. (a),(b) and (c) show the fusion weights distributions of the NetGated, ARGate-WS and ARGate+ models, respectively, when total_acc_y is corrupted. (d),(e) and (f) are the distributions of the NetGated, ARGate-WS and ARGate+ models, respectively, when total_acc_y is clean.

| # Clean Channels | Failure Model | Baseline | NetGated | ARGate-WS | ARGate+ | ARGate-L |
|------------------|---------------|----------|----------|-----------|--------------|--------------|
| All Clean | - | 94.06 | 94.50 | 94.96 | 95.69 | 96.71 |
| $n_{rclean}=8$ | Uniform | 92.35 | 92.20 | 92.45 | 92.57 | 94.06 |
| | Gaussian | 92.94 | 93.28 | 94.97 | 94.13 | 94.81 |
| $n_{rclean}=5$ | Uniform | 86.73 | 86.80 | 88.53 | 87.68 | 88.77 |
| | Gaussian | 88.41 | 89.04 | 89.52 | 90.12 | 91.35 |
| $n_{rclean}=1$ | Uniform | 62.06 | 62.90 | 65.69 | 67.09 | 69.63 |
| | Gaussian | 69.67 | 70.54 | 71.83 | 73.19 | 72.78 |

TABLE I: Prediction accuracies(in %) under clean data and random failing sensor assignment for the HAR dataset.

| # Clean Channels | Baseline | NetGated | ARGate+ | ARGate-L |
|------------------|----------|----------|---------|--------------|
| $n_{fclean}=5$ | 87.68 | 89.28 | 91.01 | 92.97 |
| $n_{fclean}=6$ | 80.59 | 81.94 | 84.52 | 89.01 |

TABLE II: Prediction accuracies(in %) under fixed failing sensor assignment for the HAR dataset.

| # Clean Channels | Baseline | NetGated | ARGate+ | ARGate-L |
|------------------|----------|----------|---------|--------------|
| (1,2)(3,8) | 72.91 | 72.75 | 77.10 | 77.16 |
| (1,3)(4,8) | 70.98 | 70.78 | 75.43 | 76.15 |
| (1,4)(5,8) | 69.38 | 69.53 | 73.06 | 73.64 |

TABLE III: Prediction accuracies(in %) under failing sensor generation test for the HAR dataset.

| # Clean Channels | Baseline | NetGated | ARGate+ | ARGate-L |
|------------------|----------|----------|---------|--------------|
| $n_{fclean}=5$ | 79.48 | 81.46 | 82.29 | 87.73 |
| $n_{fclean}=7$ | 90.39 | 92.81 | 94.56 | 95.34 |

TABLE IV: Prediction accuracies(in %) under fixed failing sensor assignment for the driver identification dataset.

| # Clean Channels | Failure Model | Baseline | NetGated | ARGate+ | ARGate-L |
|------------------|---------------|----------|----------|---------|--------------|
| All Clean | - | 95.49 | 95.79 | 96.65 | 96.78 |
| $n_{rclean}=12$ | Uniform | 93.43 | 92.19 | 93.50 | 93.58 |
| | Gaussian | 92.19 | 91.40 | 92.31 | 93.16 |
| $n_{rclean}=8$ | Uniform | 83.50 | 80.61 | 85.08 | 86.86 |
| | Gaussian | 80.82 | 79.19 | 82.23 | 85.48 |
| $n_{rclean}=5$ | Uniform | 65.36 | 62.21 | 68.96 | 73.85 |
| | Gaussian | 65.84 | 62.69 | 68.20 | 76.08 |

TABLE V: Accuracies(in %) under clean data and random failing sensor assignment for the driver identification dataset.

the baseline and NetGated by 1.29% and 0.99%, respectively. In many cases, NetGated is worse than the baseline. ARGate-L always has the best performance among all models. For example, with $n_{rclean} = 5$ and the uniform noise sensor failure model, ARGate-L significantly outperforms the baseline and NetGated by 8.49% and 13.39%, respectively.

[Failing Sensor Generation Test] We compare the generalization of two models in Table VI with the same notation of Table III. ARGate-L demonstrates noticeable improvements over all other models.

| # Failing Channels | Baseline | NetGated | ARGate+ | ARGate-L |
|--------------------|----------|----------|---------|--------------|
| (1,2)(3,15) | 60.38 | 60.39 | 59.42 | 64.16 |

TABLE VI: Prediction accuracies(in %) under the failing sensor generation test for the driver identification dataset.

D. Results on the KITTI Dataset

We compare our ARGate-L architecture to the AVOD baseline [2] on car detection in KITTI validation and test set. Average Precision (AP) in 2D image frame, oriented overlap on image, AP in BEV, and AP in 3D metrics are used for performance comparison.

In terms of validation results in Table VII, 1.17% improvement is made on 3D car detection benchmark in moderate difficulty. Furthermore, about 0.4% of improvements are found from BEV AP. With fusion weights utilized on both RPN and AVOD network, our ARGate-L architecture improves the detection performance in the validation set.

For test results evaluated by official KITTI online server, since the AVOD plane data is not provided for test set, we use our custom plane data for AVOD and ARGate-L for fair comparison. Based on this setup, in the moderate difficulty, our ARGate architecture improves 4.63% in 2D car

detection benchmark. For orientation, 4.32% improvement is observed. Lastly, for 3D detection and BEV, the proposed architecture outperforms AVOD by 4.81% and 2.22%, respectively. Furthermore, similar range of improvements are shown on the hard difficulty, which shows strength of the proposed architecture, especially on touch situation. Overall, our proposed techniques outperform the baseline AVOD rather noticeably.

| Network | Benchmark | Easy | Moderate | Hard |
|-------------|--------------------|--------------|--------------|--------------|
| AVOD | Car (3D Detection) | 84.41 | 74.44 | 68.65 |
| | Car (BEV) | 89.72 | 86.85 | 79.69 |
| AVOD-ARGate | Car (3D Detection) | 84.61 | 75.61 | 68.65 |
| | Car (BEV) | 89.95 | 87.23 | 79.89 |

TABLE VII: Average Precision (in %) comparison of car detection on the KITTI *validation* set.

| Network | Benchmark | Easy | Moderate | Hard |
|-------------|--------------------|--------------|--------------|--------------|
| AVOD | Car (Detection) | 90.17 | 79.77 | 74.84 |
| | Car (Orientation) | 89.96 | 79.19 | 74.16 |
| | Car (3D Detection) | 73.32 | 59.74 | 55.08 |
| | Car (BEV) | 88.06 | 77.80 | 71.16 |
| AVOD-ARGate | Car (Detection) | 92.36 | 84.40 | 79.59 |
| | Car (Orientation) | 92.06 | 83.51 | 78.63 |
| | Car (3D Detection) | 76.52 | 64.55 | 60.01 |
| | Car (BEV) | 87.85 | 80.02 | 75.39 |

TABLE VIII: Average Precision (in %) comparison of car detection on the KITTI *test* set.

VI. CONCLUSION

We have proposed the ARGate architectures for resilient sensor fusion by addressing the limitations of the conventional fusion schemes including the existing gating architectures. Leveraging the two proposed regularization techniques, namely, fusion weight regularization with auxiliary losses weighting, and monotonic fusion target learning, the proposed gating architectures incorporate an auxiliary model to regularize the main model to robustly learn the fusion weight for each modality. Our architectures have demonstrated significant performance improvements over other models particularly in the presence of sensor failures.

REFERENCES

- [1] Ramachandram *et al.*, “Deep multimodal learning: A survey on recent advances and trends,” *IEEE Signal Processing Magazine*, vol. 34, no. 6, pp. 96–108, 2017.
- [2] Ku *et al.*, “Joint 3d proposal generation and object detection from view aggregation,” *arXiv preprint arXiv:1712.02294*, 2017.
- [3] Chen *et al.*, “Multi-view 3d object detection network for autonomous driving,” in *IEEE CVPR*, vol. 1, no. 2, 2017, p. 3.
- [4] Wei *et al.*, “Lidar and camera detection fusion in a real-time industrial multi-sensor collision avoidance system,” *Electronics*, vol. 7, no. 6, p. 84, 2018.
- [5] Patel *et al.*, “Sensor modality fusion with cnns for ugv autonomous driving in indoor environments,” in *IROS, IEEE*, 2017.
- [6] Mees *et al.*, “Choosing smartly: Adaptive multimodal fusion for object detection in changing environments,” in *IEEE IROS*. IEEE, 2016, pp. 151–156.
- [7] Dehzangi *et al.*, “Imu-based gait recognition using convolutional neural networks and multi-sensor fusion,” *Sensors*, vol. 17, no. 12, p. 2735, 2017.

- [8] W. Zhang, H. Zhou, S. Sun, Z. Wang, J. Shi, and C. C. Loy, “Robust multi-modality multi-object tracking,” in *Proceedings of the IEEE International Conference on Computer Vision*, 2019, pp. 2365–2374.
- [9] A. Kendall, Y. Gal, and R. Cipolla, “Multi-task learning using uncertainty to weigh losses for scene geometry and semantics,” in *Proceedings of the IEEE conference on computer vision and pattern recognition*, 2018, pp. 7482–7491.
- [10] P. Gao, H. You, Z. Zhang, X. Wang, and H. Li, “Multi-modality latent interaction network for visual question answering,” in *Proceedings of the IEEE International Conference on Computer Vision*, 2019, pp. 5825–5835.
- [11] Kim *et al.*, “Robust deep multi-modal learning based on gated information fusion network,” *arXiv preprint arXiv:1807.06233*, 2018.
- [12] Anguita *et al.*, “A public domain dataset for human activity recognition using smartphones,” in *ESANN*, 2013.
- [13] Kwak *et al.*, “Know your master: Driver profiling-based anti-theft method,” in *2016 14th Annual Conference on Privacy, Security and Trust (PST)*. IEEE, 2016, pp. 211–218.
- [14] A. Geiger *et al.*, “Are we ready for autonomous driving? the kitti vision benchmark suite,” in *IEEE CVPR*, 2012.
- [15] L. Yu, C. Cuppini, J. Xu, B. A. Rowland, and B. E. Stein, “Cross-modal competition: The default computation for multisensory processing,” *Journal of Neuroscience*, vol. 39, no. 8, pp. 1374–1385, 2019. [Online]. Available: <https://www.jneurosci.org/content/39/8/1374>
- [16] B. E. Stein *et al.*, “Development of multisensory integration from the perspective of the individual neuron,” *Nature reviews. Neuroscience*, vol. 15, no. 8, pp. 520–535, 2014.
- [17] S. You *et al.*, “Deep lattice networks and partial monotonic functions,” in *NIPS*, 2017. [Online]. Available: <https://arxiv.org/abs/1709.06680>